

## Wada basins and chaotic invariant sets in the Hénon-Heiles system

Jacobo Aguirre, Juan C. Vallejo, and Miguel A. F. Sanjuán

*Nonlinear Dynamics and Chaos Group, Departamento de Ciencias Experimentales e Ingeniería, Universidad Rey Juan Carlos, Tulipán s/n, 28933 Móstoles, Madrid, Spain*

(Received 25 July 2001; published 27 November 2001)

The Hénon-Heiles Hamiltonian is investigated in the context of chaotic scattering, in the range of energies where escaping from the scattering region is possible. Special attention is paid to the analysis of the different nature of the orbits, and the invariant sets, such as the stable and unstable manifolds and the chaotic saddle. Furthermore, a discussion on the average decay time associated to the typical chaotic transients, which are present in this problem, is presented. The main goal of this paper is to show, by using various computational methods, that the corresponding exit basins of this open Hamiltonian are not only fractal, but they also verify the more restrictive property of Wada. We argue that this property is verified by typical open Hamiltonian systems with three or more escapes.

DOI: 10.1103/PhysRevE.64.066208

PACS number(s): 05.45.Ac, 05.45.Pq, 95.10.Fh

### I. INTRODUCTION

The phenomenon of chaotic scattering is usually associated with the dynamics of open Hamiltonian systems possessing chaotic properties. One of the basic attributes of these Hamiltonian systems is the possibility of an orbit to escape from the attraction of the potential. Typically, a particle bounces back and forth for a certain time in a bounded area called the *scattering region*, and eventually leaves it through one of the several exits, escaping towards infinity. Many recent studies have focused in the analysis of these Hamiltonians in two dimensions, the main reason for this interest is they are being used to model a wide range of phenomena in very different fields. Some applications are the analysis of the escape of stars from galaxies [1,2], the dynamics of ions in electromagnetic traps [3], the interaction between the Earth's magnetotail and the solar wind [4], and the study of geodesics in gravitational waves [5], to cite just a few. From a wide point of view, all these applications are varied manifestations of chaotic scattering, which mainly consists of the interaction of a particle with a system that scatters it, in a way that the final conditions of speed and direction depend on the initial conditions in an extremely sensitive way (see Ref. [6] for a detailed study of this phenomenon).

For energies below a certain threshold value, which is commonly called the *escape energy*, the orbits are bounded and the test particles cannot leave the scattering region, but if the energy is above this threshold value, several exits may appear and it is possible to escape towards infinity through anyone of them. Since we are considering a conservative Hamiltonian system, the total energy is conserved, and thus, we cannot speak about attractors nor basins of attraction. A basin of attraction is defined as the set of points that, taken as initial conditions, are attracted to a specific attractor. When there are two different attractors in a certain region of phase space, two basins exist, which are separated by a basin boundary. This basin boundary can be a smooth curve or can be instead a fractal curve. While we cannot talk about attractors in Hamiltonian systems, we can however define *exit basins* in an analogous way to the basins of attraction in a

dissipative system. In our case, an exit basin is the set of initial conditions that lead to a certain exit. In particular, we have focused our attention in the analysis of exit basins of the Hénon-Heiles Hamiltonian, which is a well-known model for an axisymmetrical galaxy [7], and it has been used as a paradigm in Hamiltonian nonlinear dynamics. It is a two-dimensional time-independent dynamical system and it has three different exits for orbits over the escape energy. It has been shown by Bleher *et al.* [8] that when two or more escapes are possible in Hamiltonian systems, fractal boundaries typically appear. Hence, the dynamics of the system is in some sense unpredictable, as the boundary that separates one basin from another one is not clearly defined.

Our goal in this paper is twofold. First, we have studied the Hénon-Heiles Hamiltonian as a paradigmatic example of chaotic scattering, paying special attention to the invariant sets related to it. Second, we have obtained numerical evidence of the special character of the final uncertainty in this Hamiltonian, because we show that its exit basins are not only fractal, but they verify the stronger property of Wada [9–14]. A basin  $B$  verifies the property of Wada if any boundary point also belongs to the boundary of two other basins. In other words, every open neighborhood of a point  $x$  belonging to a Wada basin boundary has a nonempty intersection with at least three different basins. Hence, if the initial conditions of a particle are in the vicinity of the Wada basin boundary, we will not be able to be sure by which one of the three exits the orbit will escape to infinity. It has been proved by [15] that the property of Wada is verified in a triangular configuration of three billiard balls, and it has been claimed that it could be a typical feature of chaotic scattering systems. In fact, a recent experimental evidence of the occurrence of the Wada property in chaotic scattering was reported in [17]. For a higher-dimensional case of chaotic scattering, see [16].

In this paper, we review the necessary conditions to show that a system indeed verifies the property of Wada, and we apply them to the case of the Hénon-Heiles Hamiltonian. Recent results [18,19] strongly suggest that the escape properties in two-dimensional (2D) Hamiltonians depend on generic phase-space characteristics rather than the details of

individual potentials, and they have motivated a claim for universality. Our paper is focused in this direction, supporting the claim that the Wada property is a general feature of 2D Hamiltonians with three or more escapes.

The organization of this paper is as follows. In Sec. II, we study the model and the nature of the orbits. In Sec. III, we plot the exit basins for different initial conditions. In Sec. IV, the invariant sets of the system and their dimensions are calculated, in particular, the nonattracting chaotic set formed by the orbits that will stay in the bounded region for all times, positive and negative, and its stable and unstable manifolds. We also pay attention to the average decay time. In Sec. V, we review the conditions that a Wada basin must satisfy, and apply them to our case. In particular, we calculate the only period-1 accessible boundary orbit, and we show that its unstable manifold intersects all basins. In Sec. VI, we summarize our main conclusions.

## II. DESCRIPTION OF THE MODEL

The Hénon-Heiles system was first studied by the astronomers Hénon and Heiles in 1964 [7], in the context of analyzing if there exists two or three constants of motion in the galactic dynamics. A system with a galactic potential that is axisymmetrical and time independent, possesses a 6D phase space. As there are six variables, we can find five independent conservative integrals, some of them being isolating and other nonisolating (which are physically meaningless). The question that Hénon and Heiles tried to answer is which part of this 6D phase space is filled by the trajectories of a star after very long times. By that time, it was obvious that both the total energy  $E_T$  and the  $z$  component of the angular momentum  $L_z$  were isolating integrals, while another two were usually nonisolating. Therefore, the real target became to find a third conserved quantity. In order to solve this problem, Hénon and Heiles proposed a 2D potential. Their result was that a third isolating integral may be found for only some few initial conditions. In fact, the Hénon-Heiles Hamiltonian is one of the first examples used to show how very simple systems might possess highly complicated dynamics, and since then, it has been extensively studied as a paradigm for 2D time-independent Hamiltonians.

The Hénon-Heiles Hamiltonian has a  $2\pi/3$  rotation symmetry, and it is written as

$$H = \frac{1}{2}(\dot{x}^2 + \dot{y}^2) + \frac{1}{2}(x^2 + y^2) + x^2y - \frac{1}{3}y^3. \quad (1)$$

This Hamiltonian has been extensively studied for the range of energy values below the escape energy, where orbits are bounded and a variety of chaotic and periodic motions exist. On the other hand, if the energy is higher than this threshold value, the escape energy  $E_e$ , the trajectories may escape from the bounded region and go on to infinity through three different exits. This fact can be clearly seen in Fig. 1, where its isopotential lines are plotted. Due to its symmetry properties, the exits are separated by an angle  $2\pi/3$  radians, and for the sake of clarity we call exit 1 the upper exit ( $y$

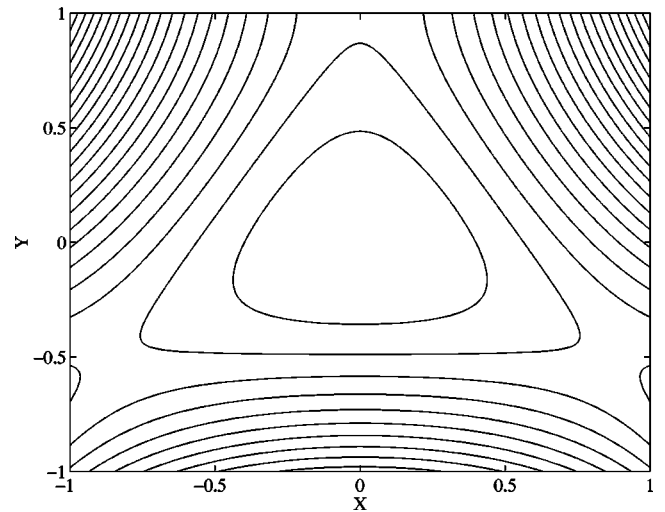


FIG. 1. Isopotential curves for the Hénon-Heiles potential. They are closed for energies under  $E_e = 1/6$ , but they show three exits if the energy is higher than this threshold value.

$\rightarrow +\infty$ ), exit 2, the left exit ( $y \rightarrow -\infty, x \rightarrow -\infty$ ), and exit 3, the right exit ( $y \rightarrow -\infty, x \rightarrow +\infty$ ).

The Hénon-Heiles potential has four terms. The first two terms  $x^2$  and  $y^2$  form a potential well, which is responsible for the oscillations of the particle, while the third and fourth terms  $x^2y$  and  $\frac{1}{3}y^3$  are responsible for the existence of the exits. In fact, the third term  $x^2y$  creates exits 2 and 3. However, it does not affect exit 1. If it disappears, then  $E_2 \rightarrow \infty$  and  $E_3 \rightarrow \infty$  and we obtain a Hamiltonian where only exit 1 is possible. On the other hand, the fourth term  $(1/3)y^3$  is only responsible for exit 1. Without it,  $E_1 \rightarrow \infty$ , exit 1 disappears and we find a chaotic scattering problem with only two symmetric escapes, exits 2 and 3.

To calculate each escape energy, it is necessary to find the value of the energy in the maxima of the potential. We obtain the same value for all three exits. There is a triangular symmetry, and  $E_1 = E_2 = E_3 = 1/6 = 0.1666$ . As we are interested in the general behavior of the two-dimensional time-independent Hamiltonians with escapes, we have only considered values of the energy above this escape energy.

In general, the particles wander to and fro for a certain time in the scattering region until they cross one of the three frontiers and escape to infinity, as it is shown in Fig. 2(a). The time they spend in the bounded region is named *escape time*. These frontiers are extremely unstable periodic orbits, known as *Lyapunov orbits* [2] [see Fig. 2(c)]. These Lyapunov orbits exist for all energies over  $E_e$ . When any orbit crosses one of them in the outer direction, that is, its velocity components pointing outwards, then the particle is forced to escape to infinity and it never comes back. As the system has three exits, there are three of these orbits.

As it can be easily understood, the higher the energy, the shorter escape times are found. However, even if the energy is high enough to allow escaping (i.e., if  $E > E_e$ ), there are several orbits that remain in the scattering region forever, being some of them periodic, some aperiodic, and some quasiperiodic [see Fig. 2(b) for the latter case].

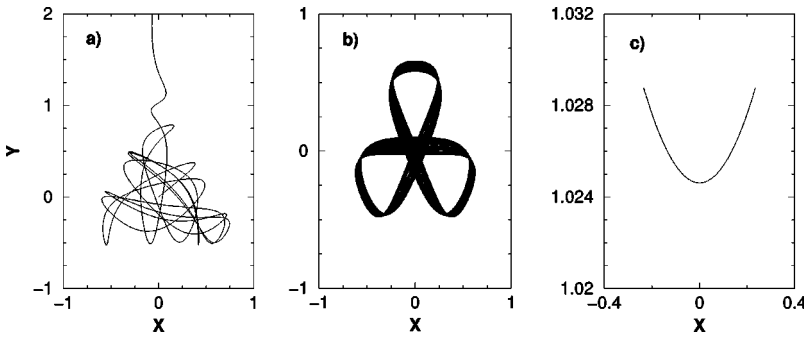


FIG. 2. Different kinds of orbits: (a) A typical escaping orbit, choosing exit 1. (b) A quasiperiodic orbit. (c) A Lyapunov orbit (LO1 for  $E = 0.25$ ).

### III. EXIT BASINS IN THE HÉNON-HEILES HAMILTONIAN

As we have mentioned before, in Hamiltonian systems, we cannot talk about attractors or basins of attraction. However, if our system has several escapes, we may define exit basins in a similar way to the basins of attraction in dissipative systems, saying that an exit basin is the set of initial conditions that lead to a certain exit. This means that we are able to construct an exit basin diagram for our system that gives us information about how the system might behave according to its initial conditions. In order to obtain the exit basin diagram for the Hénon-Heiles Hamiltonian, we must calculate each trajectory solving the differential equations of motion for a fine grid of initial conditions. We follow each orbit until it escapes from the scattering region crossing one of the three exits. If it escapes through exit 1, its initial conditions will belong to the exit 1 basin, and the same applies for exits 2 and 3. In order to visualize it, we plot each initial condition with a different color, according to the exit they have used to escape to infinity. The color code we have chosen is black for exit 1, dark gray for exit 2, and pale gray for exit 3. White represents the initial conditions that are not allowed for that particular value of the energy.

As we are studying a two-dimensional time-independent Hamiltonian, the phase space depends on  $(x, y, \dot{x}, \dot{y})$  and a conserved quantity, which is the energy. For this reason, the phase space is three dimensional, and consequently, we must fix three variables to define a trajectory. Throughout this paper, we will use a Poincaré surface of section to show our results, and the initial velocity is generically expressed by

$$v_i = \sqrt{\dot{x}^2 + \dot{y}^2} = \sqrt{2E - x_i^2 - y_i^2 - 2x_i^2 y_i + \frac{2}{3} y_i^3}. \quad (2)$$

Among the many ways of choosing the initial conditions, it is very convenient to do it in a way that includes a Lyapunov orbit. As will be seen in Sec. V, in order to demonstrate that the Hénon-Heiles Hamiltonian verifies the property of Wada, it is necessary to find an accessible unstable periodic orbit (a saddle point) and plot its associated manifolds. The Lyapunov orbits verify all these conditions. A boundary point  $P$  is *accessible* from a basin  $B$  if it is possible to draw a finite curve from an interior point in  $B$  to  $P$  in a way that it contains no boundary points but  $P$ .

The two different choices of initial conditions used to plot the exit basin diagrams are sketched in Figs. 3(a) and 3(b). It

is possible to have an exit basin diagram where the variables are  $(x, y)$ , and where the  $2\pi/3$  rotation symmetry is manifest. This choice of initial conditions is shown in Fig. 3(b), and the exit basin diagram resulting from it is plotted in Fig. 4. Apart from  $x$  and  $y$ , we have fixed the initial shooting direction for each  $(x, y)$  in a way that it is perpendicular to the radial line that goes from  $(0, 0)$  to  $(x, y)$ , in the counter-clockwise sense. Thus, the Poincaré surface of section is a map defined by the points of the trajectories that verify this condition, which is expressed by  $\vec{r} \cdot \vec{v} = 0$  ( $x\dot{x} + y\dot{y} = 0$ ) and  $(\vec{r} \times \vec{v})$  pointing in the positive sense of  $z$ -axis ( $x\dot{y} - y\dot{x}$

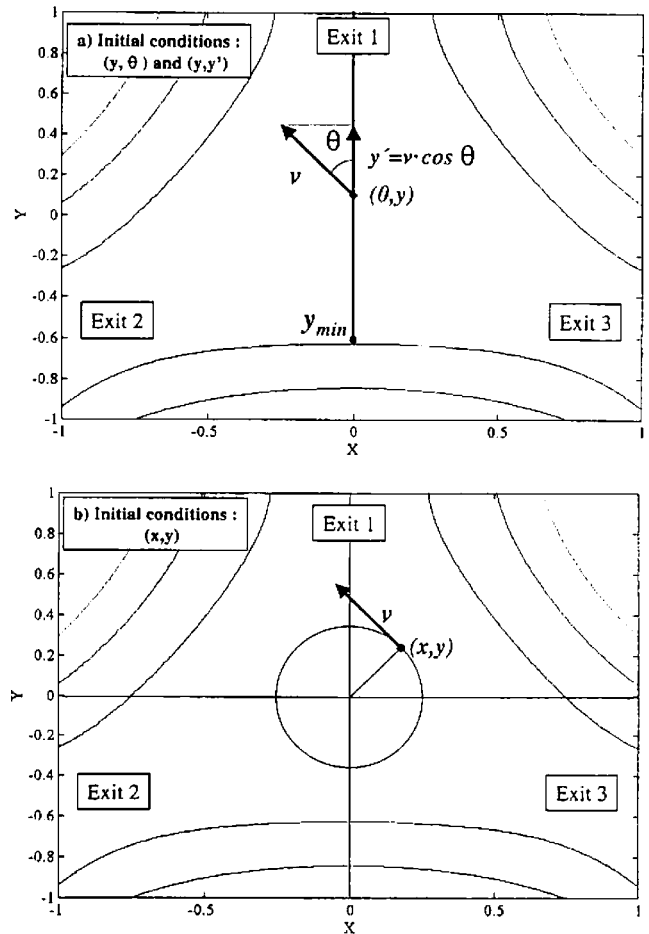


FIG. 3. Different choices for the initial conditions when plotting the exit basin diagrams. (a) Plotting  $(y, \theta)$  and  $(y, \dot{y})$ . (b) Plotting  $(x, y)$  and tangential shooting.

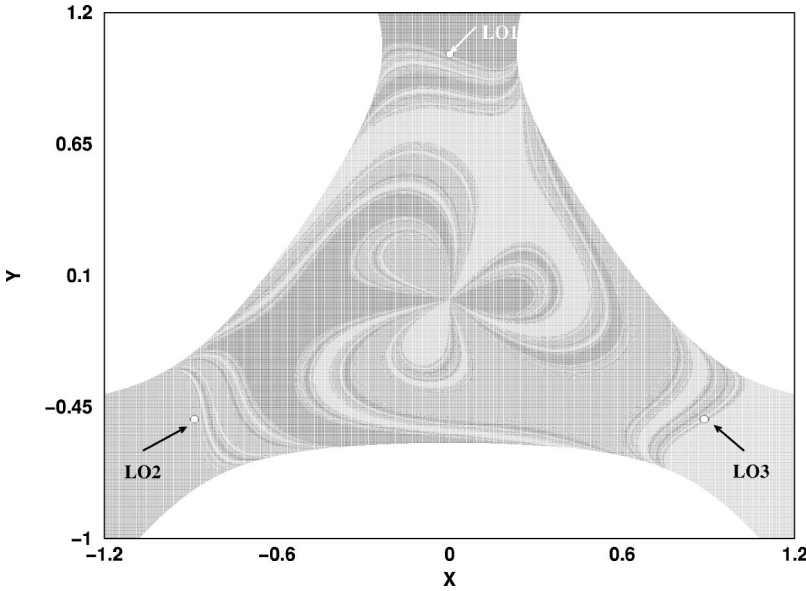


FIG. 4. Exit basin diagram with  $1000 \times 1000$  initial conditions  $(x, y)$  and  $E = 0.25$ . The initial conditions are plotted black if the orbit escapes through exit 1, dark gray for exit 2, and pale gray for exit 3. The Lyapunov orbits are remarked with arrows.

$> 0$ ). With this choice of initial conditions, all the three Lyapunov orbits (LO) are represented in the exit basin diagram (Fig. 4) and their positions are LO1,  $(0, y_{LO})$ , LO2,  $[-y_{LO}(\sqrt{2}/2), -y_{LO}(\sqrt{2}/2)]$  and LO3:  $[y_{LO}(\sqrt{2}/2), -y_{LO}(\sqrt{2}/2)]$ . The value  $y_{LO}$ , which is the distance between the origin of coordinates  $(0, 0)$  and the position of each Lyapunov orbit, depends on the energy and is calculated numerically (see Sec. V).

In order to simplify the verification of the Wada property in Sec. V, we have also calculated the exit basins for a different choice of initial conditions. They are the ones sketched in Fig. 3(a), where we can see that the fixed initial conditions are now  $x = 0, y = (y_{\min}, y > y_{LO})$  and  $\theta = (0, 2\pi)$ .  $\theta$  is the shooting angle, or in other words, the angle that  $v_i$  forms with the positive  $y$  axis, in the counterclockwise sense. The Poincaré map is defined by the plane  $x = 0$  and  $\dot{x} > 0$ , and for this choice of initial conditions, Eq. (2) becomes  $v_i = \sqrt{2E - y_i^2 + (2/3)y_i^3}$ . As the radicand must be positive, the range of allowed values of  $y_i$  is bounded from below and must be bigger than  $y_{\min}$ , where  $y_{\min}$  is the real solution of  $2E - y_i^2 + (2/3)y_i^3 = 0$ . The exit basin diagram for the choice of initial conditions  $(y, \theta)$  is shown in Fig. 5(a). The figure shows a clear mirror symmetry, and if  $(y, \theta)$  escapes through exit 2,  $(y, 2\pi - \theta)$  will escape through exit 3 and vice versa. Each initial value of  $\theta$  has a related value of initial vertical velocity  $\dot{y}_i$  expressed by  $\dot{y}_i = v_i \cos \theta$ . Therefore, we can plot the exit diagram using the choice  $(y, \dot{y})$  as initial conditions instead of  $(y, \theta)$ . We have done this in Fig. 5(b). However, in this case, there is no symmetry at all, because  $\cos \theta = \cos(\theta + \pi)$  and two different values of  $\theta_i$  correspond to one  $\dot{y}_i$ . Only the Lyapunov orbit related to exit 1 (LO1) is included in Figs. 5(a) and 5(b). Its coordinates will be  $(y_{LO}, \theta = \pi/2)$  and  $(y_{LO}, \dot{y}_i = 0)$ , where  $y_{LO}$  depends on the energy, and it is the same value as in Fig. 4.

The obtained basin boundaries are clearly fractal. We have computed several exit basin diagrams varying the value of the energy, and it is evident that for  $E = 1/6$  the fractality is

maximum, while it decreases when  $E$  gets higher, results that were first obtained in [20]. The fractal regions that occupy most of the phase space for low energies, get narrower when  $E$  increases and are difficult to recognize for  $E > 1$ , although the fractality is maintained for all values of  $E$ . The fractal dimension of the invariant sets of the Hénon-Heiles Hamiltonian will be thoroughly analyzed in the next section.

#### IV. INVARIANT SETS

Systems where chaotic motion is nonattracting are very common, and the Hénon-Heiles Hamiltonian for energies above the escape energy is a good example of this phenomenon. The invariant sets related to the Hénon-Heiles Hamiltonian give us much information about the dynamical properties of the system. We have computed the nonattracting chaotic invariant set, its stable and unstable manifold, and we have also calculated the dimensions of each set depending on the energy. Finally, we have studied the average decay time, a remarkable quantity that gives us an idea of how fast orbits escape from the scattering region, which is very much related to the dimension of the invariant sets [21].

##### A. Chaotic set and invariant manifolds

The *nonattracting chaotic set*, also known as *chaotic saddle* or *strange saddle*, is formed by a set of Lebesgue measure zero of orbits that will never escape from the scattering region for both  $t \rightarrow \infty$  or  $t \rightarrow -\infty$  [12]. Its stable manifold contains the orbits that will never escape if  $t \rightarrow \infty$ , while the unstable manifold is formed by the ones that will never escape if  $t \rightarrow -\infty$ . The orbits that constitute the chaotic set are unstable periodic orbits, of any period, or aperiodic. Furthermore, this set is formed by the intersection of its stable and unstable manifolds, each of them being a fractal set with dimension between two and three in the three-dimensional phase space. As these two manifolds are invariant sets, also their intersection is invariant, and for that reason, all orbits that start in one point belonging to the chaotic set, will never



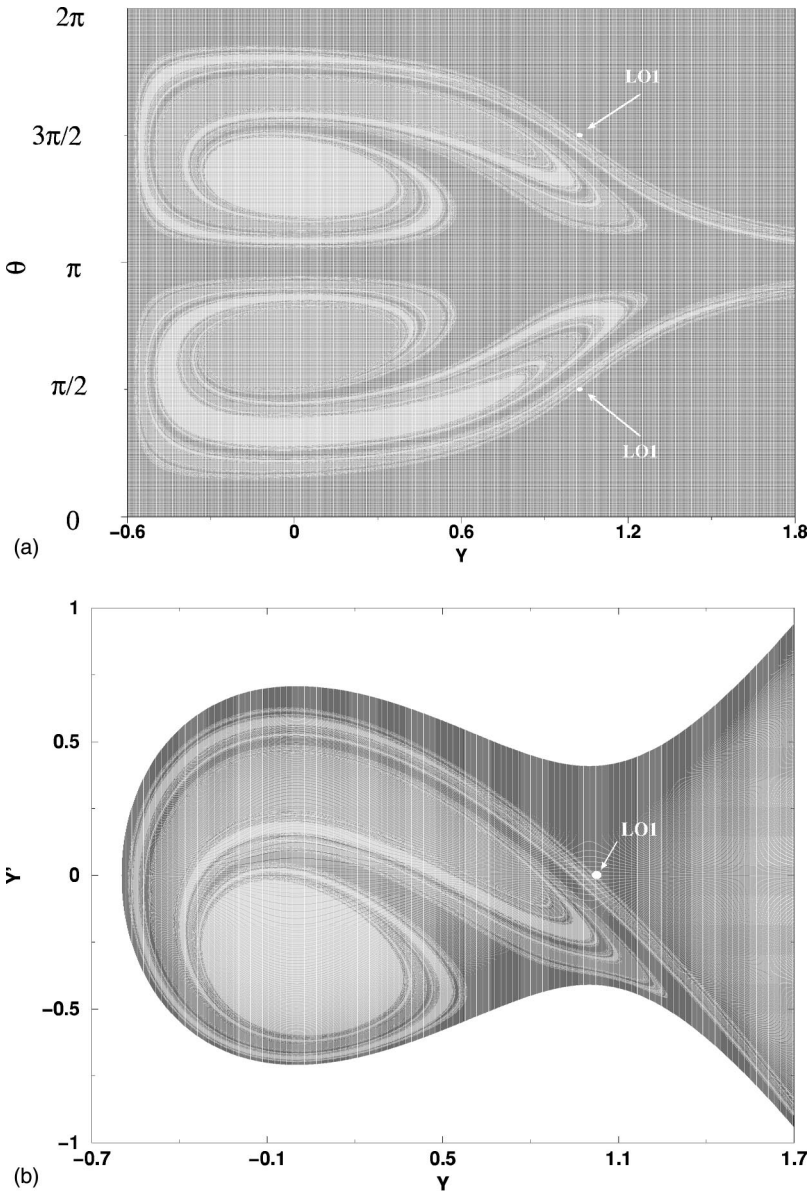


FIG. 5. Exit basin diagrams with  $1000 \times 1000$  initial conditions and  $E=0.25$ , where  $y = (y_{\min}, y > y_{LO})$  and  $\theta = (0, 2\pi)$ . The initial conditions are plotted black if their orbits escape through exit 1, dark gray for exit 2 and pale gray for exit 3. Only LO1 is defined with these initial conditions, and it is shown twice in (a) because of the symmetry of the system. (a) Initial conditions  $(y, \theta)$ . (b) Initial conditions  $(y, \dot{y})$ .

leave the set. In fact, the stable and unstable manifolds of the chaotic set are composed of the whole set of stable and unstable manifolds of each unstable point in the chaotic set.

The fractal basin boundary coincides with the stable manifold of the chaotic set, and consequently is constituted by the orbits that do not escape from the scattering region, no matter how long we wait. If an orbit is born by the boundary, the trajectory advances slowly following the stable manifold towards a saddle point of the chaotic set, spends a long time in its vicinity and it escapes to infinity following the unstable manifold. For that reason, the trajectories that are born close to the fractal boundary are the ones that spend a longer time in the scattering region. In order to obtain the stable and unstable manifold of the chaotic invariant set, as well as the chaotic set itself, we have used the “sprinkler algorithm,” which was first introduced in [22]. The main idea consists of sprinkling a large number of initial conditions from a region that contains the strange saddle. We have used a grid of  $2000 \times 2000$  points in the phase space. Then, every point is

iterated until a certain iteration  $t$ . The election of the correct value of  $t$  is not difficult, it is sufficient to find a time where most orbits have already escaped. The closer an initial point is to the stable manifold, the longer it will take to escape, and it will follow the unstable manifold to exit. Therefore, the initial points that remain in the neighborhood for a certain iteration  $t$  form the stable manifold. Their  $t$  iterations form the unstable manifold, and the iterations that are more or less in the middle between the first (stable manifold) and the last (unstable manifold) will form the chaotic set. Furthermore, the chaotic set does not depend critically on the iteration chosen to draw it. The proper interior maximum (PIM) triple method [23] is a more accurate algorithm to calculate the chaotic set, but we do not need such a high precision, so the sprinkler algorithm is enough for our purposes. This method gives nice results for the stable manifold and the strange saddle, but for the unstable manifold it is better to change the sign of every differential equation and draw the stable manifold of the dynamical system. The result will be the unstable

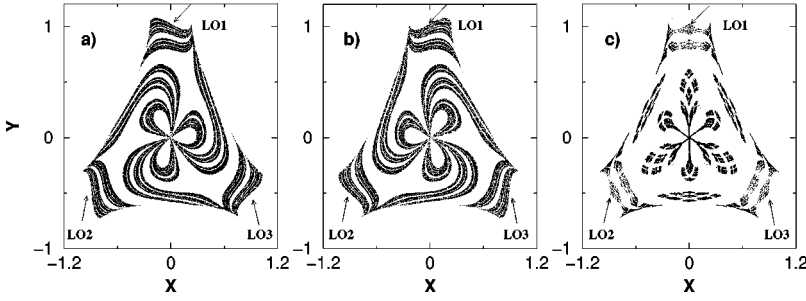


FIG. 6. Stable manifold, unstable manifold, and strange saddle for  $E=0.25$ . The initial conditions are  $(x,y)$  and tangential shooting, with a fine grid of  $2000 \times 2000$  dots. The arrows show the three Lyapunov Orbits (LO1, LO2, and LO3).

manifold of the former system. As we mentioned previously, the dimension of these fractal sets is between two and three, and so we can only plot its intersection with a Poincaré map. Obviously, these plots will depend on the choice of initial conditions defined in Fig. 3. In fact, Fig. 6 shows the Poincaré surface of section of the stable manifold, unstable manifold, and chaotic set for  $E=0.25$ , which corresponds to the exit basin diagram in Fig. 4 (see initial conditions defined in Fig. 3(b), Sec. III). In a similar way, Fig. 7 shows the same structures for  $E=0.25$ , but the Poincaré map and the initial conditions coincide with the ones defined in Fig. 3(a). The exit basin diagram related to them is the one in Fig. 5(b).

In Figs. 6 and 7, we can see that the stable manifold and the unstable manifold of the chaotic set are symmetric to each other. This is reasonable, as the Hénon-Heiles potential is conservative and invariant under time-reversal transformations ( $t \rightarrow -t, v \rightarrow -v$ ). If we compare each figure with its corresponding exit diagram [Fig. 6 with Fig. 4, Fig. 7 with Fig. 5(b)] we can see that the stable manifold really coincides with the fractal basin boundaries. It is also interesting to emphasize that the chaotic set is the intersection of a stable and an unstable manifold that are never tangent, and therefore, every saddle point is hyperbolic. The Lyapunov orbits are unstable periodic orbits, and therefore, must belong to the chaotic set. We have clearly marked them in the figures with arrows. As it was commented in Sec. III, there is only one Lyapunov orbit in Fig. 6, while Fig. 7 contains the three of them.

In order to measure the fractality of these invariant sets, we have computed the uncertainty dimension [24] for different values of the energy. Obviously, this quantity is independent of the initial conditions used to compute it. The way to do it is the following. We calculate the exit for certain initial condition  $(y, \theta)$ . Then, we compute the exit for the initial conditions  $(y + \epsilon, \theta)$  and  $(y - \epsilon, \theta)$  for a small  $\epsilon$ , and if all of them coincide, then this point is labeled as “certain.” If they do not, it will be labeled as “uncertain.” We repeat this op-

eration for different values of  $\epsilon$ . We calculate the fraction of initial conditions that lead to uncertain final states  $f(\epsilon)$ . There exists a power law between  $f(\epsilon)$  and  $\epsilon$ ,  $f(\epsilon) \propto \epsilon^\alpha$ , where  $\alpha$  is the uncertainty exponent. The uncertainty dimension  $D_0$  of the fractal set embedded in the initial conditions is obtained from the relation  $D_0 = D - \alpha$ , where  $D$  is the dimension of the phase space. If we plot  $\ln f(\epsilon)$  against  $\ln \epsilon$ , the slope will be equal to  $D - D_0$ , and we may finally obtain  $D_0$  from this value, as may be seen from

$$f(\epsilon) \propto \epsilon^{D-D_0} \Rightarrow \ln f(\epsilon) = (D-D_0) \ln \epsilon + k. \quad (3)$$

It is typical to use a fine grid of values of  $y$  and  $\theta$  to calculate the uncertainty dimension. However, this makes the algorithm very slow, and in order to solve this problem, we have fixed  $y=0$  and varied  $\theta$ . We have realized that there are no significant changes in the results as the fractality is similar in all regions of phase space, while the computing time is reduced substantially. The evolution of the exit basins when the energy is increased is shown in Fig. 8(a). The test particle is always launched from  $(x=0, y=0)$ , and the range of the shooting angles is  $\theta \in (0, 2\pi)$ . The decreasing uncertainty dimension of each invariant set for increasing energies is illustrated in Fig. 8(b), and we may compare it with the decreasing fractal structures of Fig. 8(a). As it has just been explained, the computation of the uncertainty dimension was done for only a “1D slice” of initial conditions [the vertical line  $y=0$  of Fig. 5(a)], and for that reason  $D_0 \in (0, 1)$ . According to [26],  $D_S = D_0 + N - 1 = D_0 + 2$ , where  $N$  is the dimension of the phase space ( $N=3$  in our case) and  $D_S$  is the fractal dimension of the stable manifold associated to the chaotic set. As the stable and unstable manifolds are symmetric, their fractal dimension is the same  $D_S = D_U$ . Since the invariant chaotic set is the intersection of its stable and unstable manifold, hence, its dimension is expressed by  $D_C = D_S + D_U - N = 2D_0 + 1$ .

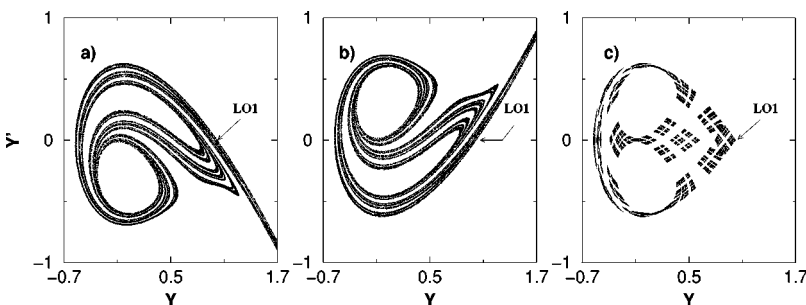


FIG. 7. Stable manifold, unstable manifold, and strange saddle for  $E=0.25$ . The initial conditions are  $(y,y)$ , with a fine grid of  $2000 \times 2000$  dots. The arrows show the only Lyapunov Orbit (LO1).

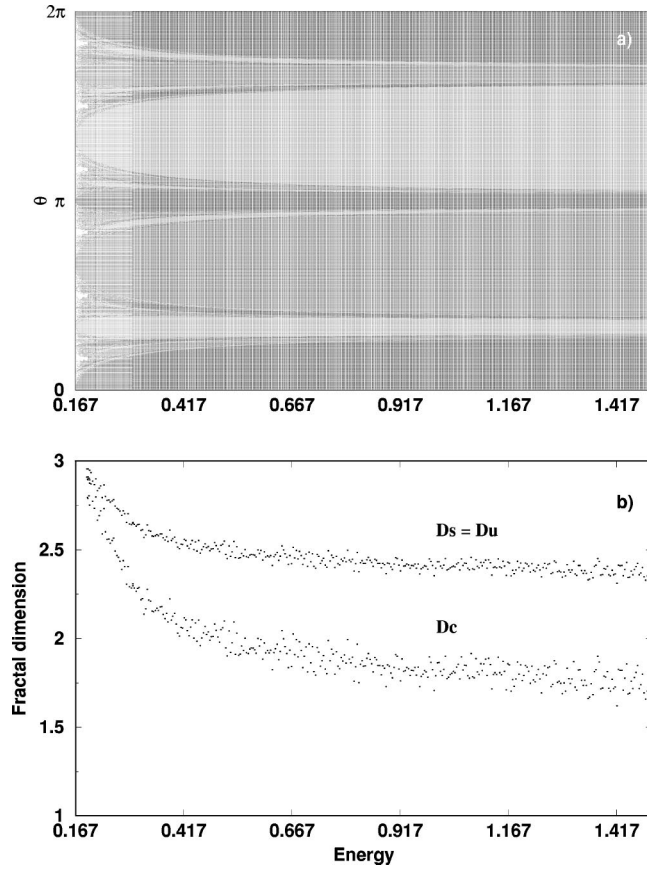


FIG. 8. (a) Evolution of the exit basin diagram for different values of the energy. The initial conditions are  $(x=0, y=0)$  and  $\theta \in (0, 2\pi)$ . Exit 1 is plotted in black, exit 2 in dark gray, and exit 3 in pale gray. (b) Fractal dimension of the invariant sets for different values of the energy:  $D_S = D_U$  for the stable and unstable manifold,  $D_C$  for the nonattracting chaotic set.

It is remarkable that the dimension of these three invariant sets tends to three, that is, the full dimension of the phase-space, when the energy tends to its minimum value  $E_e = 1/6$ . This means that for that critical value, there is a total fractalization of the phase space, and the chaotic set becomes “dense” in the limit. Consequently, in this limit there are no smooth sets of initial conditions [see Fig. 8(a)] and the only defined structures that can be recognized are the Kolmogorov-Arnold-Moser (KAM)-tori of quasiperiodic orbits, that disappear when  $E \approx 0.195$ . When the energy is increased, the different smooth sets appear and tend to grow, while the fractal structures that coincide with the boundary between basins decrease. As it was noticed in [20], the fractality remains in the Hénon-Heiles system for all  $E$ , while in many other 2D Hamiltonians it disappears when the energy reaches a certain value. In our case, the dimension of the stable and unstable manifold tends to 2.2 when  $E \rightarrow \infty$ , and therefore  $D_S = D_U \in (2.2, 3)$  (being  $D=2$  nonfractality) while the dimension of the chaotic set tends to 1.4 when  $E$  increases, and  $D_C \in (1.4, 3)$  (where  $D=1$  is nonfractality).

### B. Average decay time

One of the main consequences of nonattracting chaotic sets is the phenomenon of transient chaos [21,24,25]. An

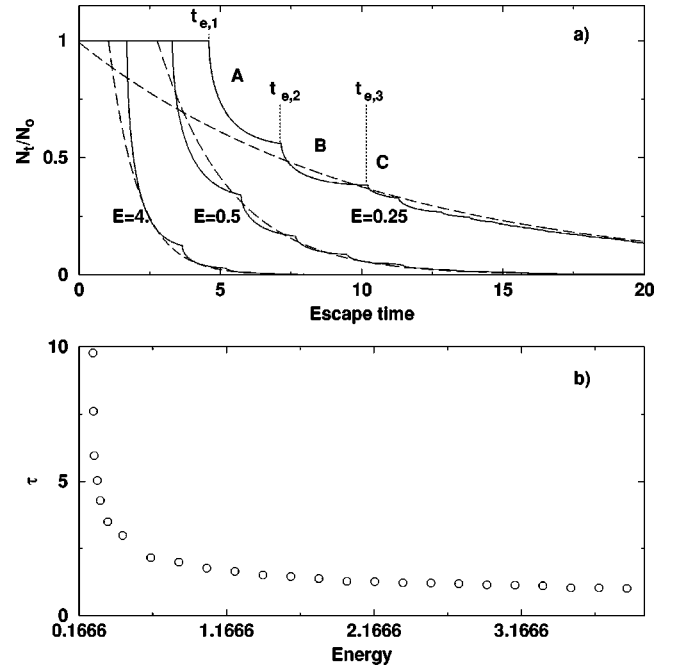


FIG. 9. (a) Fraction of remaining orbits in the scattering region in a function of the time for  $E=0.25, 0.5$ , and  $4$  (continuous line), and exponential approximation for all of them (dashed line). (b) Evolution of the average decay time  $\tau$  with the energy. It increases indefinitely when  $E \rightarrow E_e = 1/6$  from above, and tends to  $0$  when  $E \rightarrow \infty$ .

orbit may spend a long time (the escape time) orbiting in the scattering region, in the vicinity of the chaotic set, before crossing one of the three exits and escaping to infinity. During this time, its dynamics could be confused with the one of a chaotic attractor. It is usually stated that in a nonattracting chaotic system, the number of orbits that remain in the scattering region after a time  $t$  decreases exponentially. If  $1/\tau$  is the exponential decreasing rate, the *average decay time*  $\tau$  or *average transient lifetime* is expressed by

$$\frac{1}{\tau} = \lim_{t \rightarrow \infty} \frac{1}{t} \ln \left( \frac{N_0}{N_t} \right) \quad (4)$$

and consequently,

$$N_t = N_0 e^{-(t/\tau)} \quad (5)$$

for high values of time  $t$ , where  $N_0$  is the total number of initial orbits and  $N_t$  is the number of orbits remaining in the scattering region at time  $t$ . It is common, however, that the system spends a transient time  $t_0$  before any orbit escapes. In that case, Eq. (5) becomes

$$N_t = N_0 e^{-(t-t_0/\tau)} \quad (6)$$

where  $t_0$  is the time at which orbits start to escape. It is remarkable that this approximation is very precise for high  $t$ , while for low times, it is clearly unacceptable. In Fig. 9(a), we have plotted using a continuous line the fraction of remaining orbits  $(N_t/N_0)$  in function of the time  $t$  for  $E$



$=0.25, 0.5$  and  $4$ . The initial conditions are 2000 orbits with  $(x, y) = (0, 0)$  and shooting angle  $\theta = (0, 2\pi)$  [see vertical line  $y = 0$  in Fig. 5(a)]. These fractions are constant and equal to one while no orbits escape from the system. Suddenly, they start to decrease and are formed by several differentiable components separated by “peaks,” while a smooth exponential decay would be expected in a nonfractal system. The explanation of this peculiar behavior must be searched in the escape time diagram, where the escape time  $t_e$  is plotted for each initial  $\theta$  (see Ref. [20]). Every smooth (nonfractal) region of initial conditions [see Fig. 5(a)] shows a minimum in the escape time for an initial condition more or less in the center of the region, while the escape time tends to infinity in both extremes, as we reach its fractal boundary. However, each smooth region has a different minimum escape time  $t_{e,i}$ , where the regions with more initial conditions are the ones with shorter escape times. As the system has triangular symmetry, there are always three smooth regions with the same  $t_{e,i}$ , each of them composed of orbits that escape through the same exit. When the time  $t$  reaches the minimum escape time  $t_{e,1}$  for the smooth region with the lowest time escape, the orbits in that area of initial conditions start to escape and, consequently, the number of total remaining orbits in the system decreases, creating the component *A* of the curves in Fig. 9(a). In this component, it is important to remark that only orbits that started from this particular region are escaping. After a certain time, the system reaches the minimum escape time  $t_{e,2}$  for the smooth region with the second lowest time escape, and thus the curve in part *B* is the addition of the decreasing curve associated to the orbits that started in the first smooth region, plus the decreasing curve due to the orbits that started in the second smooth region and have just begun to escape. For this reason, the curves in Fig. 9(a) change their slope dramatically in  $t_{e,2}$ . In the same way, when  $t = t_{e,3}$ , the orbits that started in a certain third smooth region reach an exit, and the curves in *C* are now the addition of three different curves. This structure is repeated *ad infinitum*, as there are infinite smooth intervals of initial conditions embedded in the fractal boundary. However, after each addition, as the smooth regions that are being added own less and less orbits, the change in the slope is less prominent, and for that reason, after a few “peaks” the curves seem to be more and more regular. When  $t$  increases and more and more curves are added, the exponential approximation becomes quite precise. This fact is clearly shown in Fig. 9(a), where we have plotted the exponential approximations (dashed lines) over each of the three curves. Surprisingly, the cases with the lowest energy are the ones with worst approximation for low times, but best exponential fittings. Certainly, the approximation for the curve related to  $E = 0.25$  is almost indistinguishable from the real one after  $t \approx 20$ .

In order to calculate  $\tau$ , the usual method is based on counting how many orbits remain for different values of time  $t$ . As the relation between  $N_0$  and  $N_t$  must be exponential, it is possible to linearize Eq. (6) in the decreasing regime (after  $t_0$ ) and obtain

$$\ln \frac{N_0}{N_t} = \frac{t - t_0}{\tau} = mt + c, \quad (7)$$

where  $m$  is the slope and  $c$  the intercept in the linear regression. Therefore, we can obtain  $\tau$  and  $t_0$  from the simple expressions  $\tau = 1/m$  and  $t_0 = -c/m$ , and use them to plot the approximations shown in Fig. 9(a).

In Fig. 9(b), we have plotted  $\tau$  for different values of the energy  $E$ . As expected, the main features of this dependence are that  $\tau$  is infinitely high for  $E = 1/6$ , when test particles bounce around slowly and indefinitely, and decays to 0 when  $E$  tends to infinity and the test particles move and escape extremely fast.

## V. BASINS OF WADA

The main goal of this paper is to show that the exit basins of the Hénon-Heiles Hamiltonian and other related chaotic scattering problems are not only fractal, but they also verify the property of Wada. Although it is hard to imagine, it is possible to have three or more regions sharing the same boundary. Usually, three regions in two dimensions, for example, three countries, may only coincide in one point, but topologically, this is not necessarily true for open sets. If we talk about basins, a basin *B* verifies the property of Wada if any initial condition that is on the boundary of one basin is also simultaneously on the boundary of three (or more) basins. In other words, every open neighborhood of a point  $x$  belonging to a Wada basin boundary has a nonempty intersection with at least three different basins. The first example of a system with this property was given by Yoneyama in 1917 [27], who attributed it to Wada, from whom it took the name. The “Lakes of Wada” are a useful example of how to construct three regions that verify this condition, and they are widely explained in [9]. Logically, the boundaries of these sets must verify unusual topological properties. Topologically, the Wada property is associated to the concept of indecomposable continuum [9,28–30]. Such indecomposable sets are compact, metric, and connected sets with the strange property that when one attempts to divide them into two pieces, they split up into infinitely many pieces. Therefore, if a dynamical system verifies the property of Wada, the unpredictability is even stronger than if it only had fractal basin boundaries. If a trajectory starts close to any point in the boundary, it will not be possible to predict its future behavior, as its initial conditions could belong to any of the three basins. This particular property is verified by several dynamical systems, such as the forced damped pendulum or the Hénon map for certain values of the parameters [9,10].

The study of 2D Hamiltonians recently has attracted the interest of numerous scientists from different disciplines. It has been shown that the existence of fractal basin boundaries is typical in them [8], and Poon *et al.* [15] proved that they are indeed Wada in a billiard problem. In this sense, we have obtained numerical evidence that confirms that the Wada property is verified by the Hénon-Heiles Hamiltonian, and we conjecture that it is a general property of other related two-dimensional time-independent Hamiltonians with escapes, very widely used in the modelization of astrophysical systems.



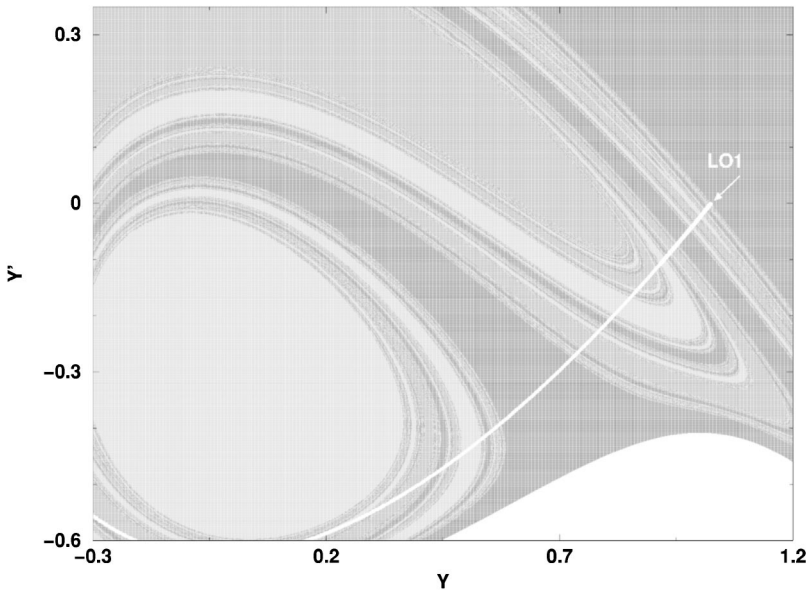


FIG. 10. The unstable manifold of the only accessible unstable periodic orbit (LO1) crosses all the basins in this zoom of Fig. 5(b). Therefore, the Hénon-Heiles Hamiltonian verifies the property of Wada.

### A. Computational conditions to verify the Wada property

Although it might be easy to visualize from an intuitive point of view whether or not a dynamical system verifies the Wada property, the numerical verification presents several difficulties that must be solved, as the topology behind this property is not trivial. A thorough analysis of this subject was done in [9,10], and some computational conditions were found to assure that a basin is Wada, which for the sake of clarity we sketch in the following:

*a. Main condition:* Let  $P$  be an unstable periodic orbit, accessible from a basin  $B$ . It must be verified that its unstable manifold intersects every basin.

*b. Secondary conditions:* If such a saddle point exists, the basin  $B$  verifies the property of Wada if any of the following next points are true:

- (1) The stable manifold of the saddle point  $P$  is dense in the boundary of the three regions.
- (2) The periodic orbit  $P$  is the only accessible orbit from basin  $B$ . In case there exists more than one accessible periodic orbit, every unstable manifold must intersect all basins (Theorem 1 of [10]).
- (3) The periodic orbit  $P$  generates a basin cell (Theorem 2 of [10]).

The *basin cells* were first introduced by Nusse and Yorke [10]. However, before introducing the concept of a basin cell, it is necessary to define a *trapping region*. A trapping region  $A$  is a compact region formed by initial conditions that, after iterations, become a different region  $B$  that belongs to  $A$  and is smaller than  $A$ . Formally,  $A$  is a trapping region  $\Leftrightarrow F(A) \subset A$  and  $F(A) \neq A$ . Therefore, if the particle enters the trapping region, it will never be able to escape from it. A basin cell is a trapping region constructed in a way that its boundary is made out of  $n$  pieces of stable and unstable manifolds of a  $n$ -periodic orbit that also lies on the boundary of the trapping region.

### B. Verification of the Wada property

In order to do all the computations and show the results in the simplest way, we make the choice of initial conditions  $(y, \dot{y})$ , although the conclusions are extensible to any other choice. Therefore, the initial conditions are the ones defined in Fig. 3(a), and the exit basin diagram is the one shown in Fig. 5(b). Recall that for this particular choice, only the Lyapunov orbit related to exit 1 (the upper one) is plotted [see Fig. 5(b)]. As it has been sufficiently explained, an accessible unstable periodic orbit is needed. The period-1 Lyapunov orbit related to exit 1 fulfills this condition, and hence, we compute it with very high precision. As can be seen in Fig. 2, LO1 is symmetric with respect to the  $y$  axis. For that reason, we know that just when  $x=0$  the trajectory must be perpendicular to the  $y$  axis (tangent slope zero), and so the initial value for  $\dot{y}$  is known without any ambiguity and equal to 0. As the phase space variables are  $(y, \dot{y})$ , the LO1 coordinates are  $y_{LO} = f(E)$ ,  $\dot{y} = 0$ . Therefore, it would be necessary to find the relation between  $y_{LO}$  and the value of the energy, but for our purposes, it is enough to have it for a certain energy. We have computed it for  $E=0.25$ , and the result is  $y_{LO} = 1.024\,611\,462\,679$ . We have computed it with twelve digits, since the algorithm used later to calculate its stable and unstable manifolds requires very high precision. Several authors have used quadruple precision for calculating LO in very similar Hamiltonians [2], but our aim is to draw part of its unstable manifold, and for this purpose, double precision is enough. This orbit is accessible by construction, as we are sure that if instead of the  $y_{LO}$  value for LO1 we had  $y_{LO} + \varepsilon$ , (with the same  $\dot{y} = 0$ ) the particle would clearly belong to basin 1, escaping through exit 1, and not even being able to enter the scattering region [see Fig. 5(b)]. For the same reason, if instead of  $\dot{y} = 0$ , we had  $\dot{y} = \varepsilon$ , the particle would be shot towards outside of the scattering region, and therefore it would never return.

In order to draw the stable and the unstable manifold of  $P$  (LO1), we use the algorithm explained in [31] based on plot-

ting several iterations of points very close to  $P$  in the direction of the eigenvectors. We show in Fig. 10, that the Hénon-Heiles Hamiltonian verifies the first and basic hypothesis, as the unstable manifold of an accessible periodic orbit indeed crosses all three basins. However, although this fact is a strong point in favor of our assumption, we should check conditions 1, 2, or 3. Unfortunately, this is not an easy task, as it is computationally very difficult to authenticate any of them. First of all, it is hard to confirm that the unstable manifold is dense (condition 1) using computational tools, and it is already shown with a similar system in [15]. On the other hand, it is even more complicated to assure that our periodic orbit is the only one accessible from basin 1 (condition 2). We can find as many periodic orbits as we want, but we will never be absolutely sure that we have not lost any in the numerical search, specially for very high periods. Finally, it is not possible to build a basin cell with the invariant manifolds of  $P$ , as we are not working with attractors and the manifolds do not cross as we would like to. The “attractors” are now in the infinity, where  $y = \infty$  and  $\dot{y} = \infty$ . What we see is that the unstable manifold twice intersects the same branch of the stable manifold, but never the other one, and this is a necessary condition to create a basin cell. In summary, this is only possible for dissipative systems.

Both conditions 1 and 2 are possible, and we have decided to work with the latter, showing that LO1 is the only unstable periodic orbit that is also accessible from the exit 1 basin. We use an argument based on [32], where it is proved that if all the periodic points in the boundary of a basin are hyperbolic, and there exists an accessible periodic point of minimum period  $q$ , then every accessible point in the basin boundary either is a periodic point of minimum period  $q$  or is in the stable manifold of such a periodic point. From here, we may assume that in our boundary, only period-1 orbits may be found. This theorem provides us with a very powerful tool to verify condition 2, as there are no big problems in finding period-1 orbits in the boundary of basin 1. A few periodic orbits for  $E = 0.25$  have been found, although none of them were in the boundary. Therefore, we have obtained enough numerical evidence to affirm that basin 1, formed by the initial conditions of the orbits that escape towards  $y \rightarrow \infty$ , satisfies the property of Wada. For the other two basins, the same reasoning can be followed, as the Hénon-Heiles Hamiltonian has a  $2\pi/3$  symmetry. The only difference would be to change the initial conditions in a way that the new  $y$  axis forms a  $2\pi/3$  angle with the former one, and therefore contains a different Lyapunov orbit.

## VI. CONCLUSIONS

In this paper, we have studied in detail the dynamics of the Hénon-Heiles Hamiltonian in the range of energy values higher than the escape energy  $E_e = 1/6$ , where consequently, exits are present. We have analyzed the different nature of the orbits and paid special attention to the computation of the exit basin diagrams, which show a rich pattern of fractal structures. As an important ingredient of our paper, the invariant sets associated to the system have received considerable attention. In particular, computations of the stable and unstable manifolds, and the chaotic saddle, which is the intersection of the invariant manifolds, have been carried out. Since they are fractal sets, we have calculated the corresponding fractal dimensions for different values of the energy. Moreover, we have calculated the average decay time, as a useful tool to characterize how fast orbits escape from the scattering region. We have found that the number of orbits that remain in the bounded region depends on time in a very particular way, showing a curve formed by infinite decreasing intervals, each of them depending on every smooth part of a basin, and it decreases exponentially only when the time  $t$  gets large enough. The main conclusion of this paper has been to show that the Hénon-Heiles system possesses Wada basins, meaning that any initial condition that is on the boundary of a basin, is also simultaneously on the boundary of the other two basins. Furthermore, a detailed summary of the conditions to be verified for a system to have the Wada property is presented. We believe it may be useful as a general procedure for conservative and dissipative systems. Finally, we would like to point out that interesting aspects of this problem are still open, such as a detailed analysis of the abrupt transition at the escape energy, and a simpler formulation of the conditions to be verified for a Hamiltonian system to possess the Wada property, even for higher dimensions.

## ACKNOWLEDGMENTS

We would like to thank James A. Yorke, George Contopoulos, Erik Kostelich, and Elbert E. Macau for the fruitful talks we have had with them during the development of this research. This work has been supported by the Spanish DGES under Project No. PB96-0123 and by the Spanish Ministry of Science and Technology under Project No. BFM2000-0967.

- 
- [1] G. Contopoulos, H. E. Kandrup, and D. Kaufman, *Physica D* **64**, 310 (1993).  
 [2] G. Contopoulos, *Astron. Astrophys.* **231**, 41 (1990).  
 [3] G. Z. K. Horvath, J. L. Hernández Pozos, K. Dholakia, J. Rink, D. M. Segal, and R. C. Thompson, *Phys. Rev. A* **57**, 1944 (1998).  
 [4] J. Chen, J. L. Rexford, and Y. C. Lee, *Geophys. Res. Lett.* **17**, 1049 (1990).

- [5] K. Veselý and J. Podolský, *Phys. Lett. A* **271**, 368 (2000).  
 [6] S. Bleher, C. Grebogi, and E. Ott, *Physica D* **46**, 87 (1990).  
 [7] M. Hénon and C. Heiles, *Astron. J.* **69**, 73 (1964).  
 [8] S. Bleher, C. Grebogi, E. Ott, and R. Brown, *Phys. Rev. A* **38**, 930 (1988).  
 [9] J. Kennedy and J. A. Yorke, *Physica D* **51**, 213 (1991).  
 [10] H. E. Nusse and J. A. Yorke, *Physica D* **90**, 242 (1996).  
 [11] H. E. Nusse and J. A. Yorke, *Science* **271**, 1376 (1996).

- [12] K. T. Alligood, T. D. Sauer, and J. A. Yorke, *Chaos, An Introduction to Dynamical Systems* (Springer-Verlag, New York, 1997).
- [13] H. E. Nusse, E. Ott, and J. A. Yorke, *Phys. Rev. Lett.* **75**, 2482 (1995).
- [14] H. E. Nusse and J. A. Yorke, *Phys. Rev. Lett.* **84**, 626 (2000).
- [15] L. Poon, J. Campos, E. Ott, and C. Grebogi, *Int. J. Bifurcation Chaos Appl. Sci. Eng.* **6**, 251 (1996).
- [16] Z. Kovács and L. Wiesenfeld, *Phys. Rev. E* **63**, 056207 (2001).
- [17] D. Sweet, E. Ott, and J. A. Yorke, *Nature (London)* **399**, 315 (1999).
- [18] C. Siopis, H. E. Kandrup, G. Contopoulos, and R. Dvorak, *Celest. Mech. Dyn. Astron.* **65**, 57 (1997).
- [19] H. E. Kandrup, C. Siopis, G. Contopoulos, and R. Dvorak, *Chaos* **9**, 381 (1999).
- [20] A. P. S. de Moura and P. S. Letelier, *Phys. Lett. A* **256**, 362 (1999).
- [21] G.-H. Hsu, E. Ott, and C. Grebogi, *Phys. Lett. A* **127**, 199 (1988).
- [22] H. Kantz and P. Grassberger, *Physica D* **17**, 75 (1985).
- [23] H. E. Nusse and J. A. Yorke, *Physica D* **36**, 137 (1989).
- [24] E. Ott, *Chaos in Dynamical Systems* (Cambridge University Press, Cambridge, 1993).
- [25] T. Tél, "Transient Chaos," in *Directions in Chaos, Vol. 3, Experimental Study and Characterization of Chaos*, edited by Hao Bai-Lin (World Scientific, Singapore, 1990), pp. 149–211.
- [26] Y-C Lai, A. P. S. de Moura, and C. Grebogi, *Phys. Rev. E* **62**, 6421 (2000).
- [27] K. Yoneyama, *Tohoku Math. J.* **11-12**, 43 (1917).
- [28] M. A. F. Sanjuán, J. Kennedy, C. Grebogi, and J. A. Yorke, *Chaos* **7**, 125 (1997).
- [29] M. A. F. Sanjuán, J. Kennedy, E. Ott, and J. A. Yorke, *Phys. Rev. Lett.* **78**, 1892 (1997).
- [30] J. Kennedy, M. A. F. Sanjuán, J. A. Yorke, and C. Grebogi, *Top. Appl.* **94**, 207 (1999).
- [31] Z. You, E. J. Kostelich, and J. A. Yorke, *Int. J. Bifurcation Chaos Appl. Sci. Eng.* **1**, 605 (1991).
- [32] K. T. Alligood and J. A. Yorke, *Ergod. Th. & Dynam. Sys.* **12**, 377 (1992).